Fast ^{19}F Magic-Angle-Spinning NMR Crystallography for Structural Characterization of Fluorine-Containing Pharmaceutical Compounds

Changmiao Guo[1,2], **Matthew Fritz**[1,2], **Jochem Struppe**[4], **Sebastian Wegner**[5], **John Stringer**[6], **Ivan V. Sergeyev**[4], **Caitlin M. Quinn**[1], **Angela Gronenborn**[2,3,*], **Tatyana Polenova**[1,2,*]

[1]Department of Chemistry and Biochemistry, University of Delaware, Newark, Delaware 19716, United States

[2]Pittsburgh Center for HIV Protein Interactions, University of Pittsburgh School of Medicine, 1051 Biomedical Science Tower 3, 3501 Fifth Avenue, Pittsburgh, Pennsylvania 15261, United States

[3]Depadment of Structural Biology, University of Pittsburgh School of Medicine, 3501 Fifth Ave., Pittsburgh, PA 15261, United States

[4]Bruker Biospin Corporation, 15 Fortune Drive, Billerica, Massachusetts 01821, United States

[5]Bruker BioSpin GmbH, Rheinstetten, Germany

[6]PhoenixNMR, 510 E. 5th Streest, Loveland, CO 80537, United States

Abstract

Fluorine-containing compounds comprise twenty to thirty percent of all commercial drugs, and the proportion of fluorinated pharmaceuticals is rapidly growing. While magic angle spinning (MAS) NMR spectroscopy is a popular technique for analysis of solid pharmaceutical compounds, fluorine has been underutilized as a structural probe so far. Here we report a fast (40 kHz) MAS ^{19}F NMR approach for structural characterization of fluorine-containing crystalline pharmaceutical compounds at natural abundance, using the antimalarial fluorine-containing drug mefloquine as an example. We demonstrate the utility of 2D [19]F-^{13}C and [19]F-^{19}F dipolar-

*Corresponding authors: Tatyana Polenova, Department of Chemistry and Biochemistry, University of Delaware, Newark, DE, USA, Tel.: (302) 831-1968; tpolenov@udel.edu; Angela M. Gronenborn, Department of Structural Biology, University of Pittsburgh School of Medicine, 3501 Fifth Ave., Pittsburgh, PA 15260, USA, Tel.: (412) 648-9959; ama100@pitt.edu.

CONFLICT OF INTEREST
The authors declare no conflict of interest.

SUPPORTING INFORMATION
1D [19]F-^{13}C CPMAS spectra of mefloquine acquired at various Hartmann-Hahn matching conditions; ^{13}C chemical shift assignments from DFT calculations and [1]H-^{13}C CPMAS spectra; 2D [19]F-^{13}C HETCOR spectra acquired at various conditions; 2D [19]F-^{19}F RFDR spectrum and representative 1D traces; ^{19}F spectra with selective DANTE excitation and inversion pulses applied at different frequencies; 1D ^{19}F DANTE-RFDR spectra acquired with various RFDR mixing times; experimental and simulated ^{19}F DANTE-RFDR magnetization exchange curves for 2CF$_3$ and 8CF$_3$ groups; SNR for different [19]F-^{13}C CP conditions; intra- and intermolecular [19]F-^{19}F distances in the crystal structure; an example script for DANTE-RFDR multispin simulations. This information is available online at http://pubs.acs.org.

coupling-based correlation experiments for ^{19}F and ^{13}C resonance frequency assignment, which permit identification of crystallographically inequivalent sites. The efficiency of ^{19}F-^{13}C cross-polarization (CP) as well as the effect of ^{1}H and ^{19}F decoupling on spectral resolution and sensitivity were evaluated in a broad range of experimental conditions. We further demonstrate a protocol for measuring accurate interfluorine distances based on 1D DANTE-RFDR experiments combined with multi-spin numerical simulations.

Abstract Graphic:
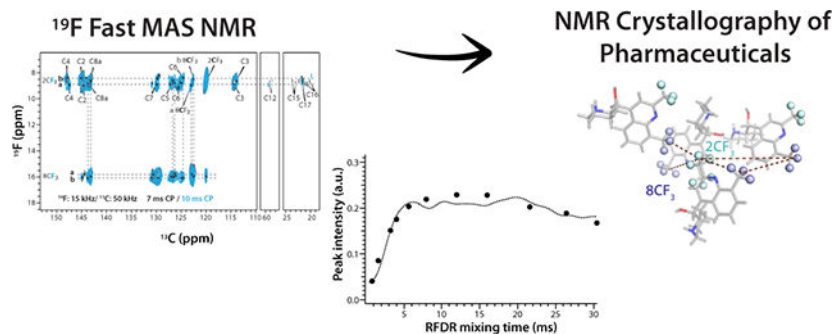
Keywords

fast ^{19}F MAS NMR; ^{19}F-^{13}C heteronuclear correlations; ^{19}F decoupling; F-F RFDR; interfluorine distances; mefloquine

INTRODUCTION

Fluorinated compounds are becoming increasingly dominant in medicinal chemistry[1]. Fluorine-containing molecules comprise 20% of all pharmaceuticals and 30% of newly approved drugs[2–4], and according to current estimates, over 150 commercial drugs contain fluorine atoms or fluoroalkyl groups, including several of the most-prescribed and/or most-profitable on the market[2–4]. Structural characterization of pharmaceuticals relies on crystallography and NMR spectroscopy; fluorine NMR is becoming increasingly important in this regard. ^{19}F is a 100% naturally abundant spin 1/2 nucleus and possesses a high gyromagnetic ratio, making it a very attractive probe for NMR applications. ^{19}F resonance frequencies are also exquisitely sensitive to the local structural and electronic environment around the fluorine nuclei, exhibiting a chemical shift range of over 300 ppm[5,6].

While ^{19}F NMR has been extensively applied in the analysis of fluorinated organic and biological molecules in solution[7–13], MAS NMR studies remain relatively scarce[14–26]. This, in part, is due to i) strong dipolar couplings that result in broad lines, requiring high-power ^{1}H and ^{19}F decoupling with specialized hardware, and ii) relatively low sensitivity in heteronuclear polarization transfer experiments in the common regime of magic angle spinning (MAS) frequencies, below 30 kHz. Increasing the MAS frequencies to 40 kHz and above results in significant improvements in sensitivity and resolution[24–26], yielding substantially narrowed ^{19}F lines, even in the absence of ^{1}H decoupling[19,20,25]. Furthermore, homonuclear ^{19}F-^{19}F recoupling experiments, such as 2D radio frequency driven recoupling

(RFDR) and delays alternating with nutation for tailored excitation (DANTE)-RFDR, are effective and can be used for interfluorine distance measurements, including in multi-spin systems[15,18,19,24]. In particular, long-range ^{1}H-^{19}F and ^{19}F-^{19}F interatomic distances[27] together with ^{19}F-^{13}C contacts,[13,21,28,29] are indispensable parameters[30] in structure elucidations.

Here we report on a fast MAS ^{19}F NMR crystallography approach for structure determination of crystalline fluorine-containing pharmaceutical compounds at natural abundance. This integrated approach was developed by us for structural analysis of active pharmaceutical ingredients and provides detailed information on the 3D structure. Our methodology was established using the antimalarial drug mefloquine[31] (Fig. 1) whose X-ray structure is known. Combining 2D homonuclear ^{19}F-^{19}F and heteronuclear ^{19}F-^{13}C dipole-coupling-based experiments with Density Functional Theory (DFT) calculations, complete assignments of ^{19}F and ^{13}C chemical shifts were obtained, revealing three crystallographically inequivalent fluorine sites in the unit cell of mefloquine. We show that at MAS frequencies of 40 kHz and above, low-power double-quantum cross polarization (CP) is optimal for achieving high ^{19}F-^{13}C polarization transfer efficiencies and for recording short- and long-range ^{19}F-^{13}C correlations. The effects and the efficiency of ^{1}H and ^{19}F decoupling on ^{19}F-^{13}C heteronuclear correlation (HETCOR) spectra were evaluated and a comprehensive analysis of multi-spin effects was performed. Magnetization exchange curves recorded in DANTE-RFDR experiments allowed us to extract accurate intra- and intermolecular fluorine-fluorine distances.

It is well known that polymorphs and solvates can impact the therapeutic performance for certain drugs,[32] and patenting new polymorphs after the original drug is a common strategy for extending drug commercial lifecycle.[33] The fast MAS ^{19}F NMR crystallography approach, exemplarily demonstrated herein for crystalline mefloquine, allows for quick and efficient characterization of polymorphs. We envision that it will be broadly adopted for analysis of active pharmaceutical ingredients in pharmaceutical formulations of unknown structures.

RESULTS

^{19}F MAS NMR Spectra: MAS Frequency and Decoupling

^{19}F MAS spectra of mefloquine acquired at MAS frequencies of 10, 40, and 60 kHz are shown in Fig. 2. Very strong signals emerge in only a single scan, and the signal-to-noise ratios (SNR) for spectra acquired with 32 scans at MAS frequencies of 10, 40, and 60 kHz, without and with ^{1}H decoupling, are remarkably high: 307/561, 1215/1655, 1535/2120, respectively. At a MAS frequency of 10 kHz, a manifold of 8 spinning sidebands was observed for each of the two broad peaks with isotropic chemical shifts of 16.2 and 8.8 ppm. The corresponding line widths for the center bands are 922 and 745 Hz in the absence of ^{1}H decoupling. When ^{1}H Spinal-64 decoupling at an RF B_1 field of 90 kHz was applied, the lines became somewhat narrower, 843 and 317 Hz, respectively. The upfield resonance exhibited asymmetric lineshape but remained unresolved. The ^{19}F T_1 are 1.4 s and 2.5 s for the downfield and upfield peaks, respectively, while ^{1}H T_1 are 4.7–5.0 s.

The spectra at 40 kHz and 60 kHz provided in Fig. 2 reveal 5 distinct resonances, with isotropic chemical shifts of 16.2 ppm, 15.9 ppm (a shoulder), 15.6 ppm, 8.8 ppm, and 8.2 ppm. Dramatic improvements in resolution are seen when increasing the MAS frequencies to 40 and 60 kHz. At 40 kHz, the line widths of the downfield and upfield resonances are 440 and 230 Hz without decoupling; with ^{1}H SW_f-TPPM decoupling at the RF field of 10 kHz, those are 378 and 143 Hz, respectively. At 60 kHz without ^{1}H decoupling, the line widths are 322 and 171 Hz; those in the presence of 15 kHz ^{1}H SWf-TPPM are 300 and 117 Hz, respectively. Taken together, these results unequivocally demonstrate that fast MAS frequencies are critical from both sensitivity and resolution, and that, even at 60 kHz, ^{1}H decoupling is necessary. Conversely, even with high-power (90 kHz) ^{1}H decoupling, the resolution is very poor at 10 kHz MAS and the SNR is 4-fold lower than at 60 kHz MAS.

[19]F-[13]C Cross-Polarization: Optimal Conditions for Fast MAS Experiments

[1]H-^{13}C and [19]F-^{13}C CPMAS spectra of mefloquine are shown in Fig. 3. All carbon resonances are detected in the [1]H-^{13}C CPMAS spectrum (Fig. 3a) as well as the non-^{1}H decoupled [19]F-^{13}C spectrum (Fig. 3b), except for C14, which is farthest away from the two CF_3 groups. In the [19]F-^{13}C CPMAS experiments, the polarization transfer efficiency between fluorine and the aromatic carbons is similar to that in the [1]H-^{13}C CPMAS experiment, with a 0.6 signal-to-noise ratio (SNR) per square root of scans.

Effects and efficiency of ^{1}H and ^{19}F decoupling was evaluated for different decoupling sequences (Fig. 3b–d). For fluorine decoupling, high-power π-pulses were introduced every rotor period[34] and proton decoupling employed the low power XiX scheme[35], applied simultaneously with fluorine decoupling. Fluorine decoupling (Fig. 3c) increased the signal intensity and narrowed the CF_3 carbon resonances, as expected. At the same time, with only fluorine decoupling, non-CF_3 carbon signal intensities are reduced by different degrees relative to the [1]H-decoupled spectra. When proton and fluorine decoupling is applied simultaneously (Fig. 3d), the spectrum exhibits improved resolution throughout.

[19]F-^{13}C polarization transfer efficiencies were assessed by recording CPMAS spectra for different Hartmann-Hann matching conditions with radiofrequency (rf) fields varied from 5 kHz to 120 kHz. Both double-quantum (DQ) and zero-quantum (ZQ) conditions were examined. We found that several DQ and ZQ conditions led to efficient CP transfers for 15 kHz or 35 kHz ^{19}F radio frequency (rf) fields. DQ transfers appear to be more efficient than their ZQ counterparts, with the low-power CP transfers considerably more efficient than the high-power conditions (Fig. S1 and Table S1 of the Supporting Information). The highest transfer efficiency was achieved for first-order DQ CP with 15 kHz ^{19}F and 25 kHz ^{13}C rf fields (Fig. S1, Fig. S2a–b).

In addition, [19]F-^{13}C CPMAS spectra were recorded with different contact times, to obtain magnetization buildup profiles for different resonances. Contact times of 6 ms or higher are necessary to cross-polarize the aliphatic carbons while intensities for the aromatic carbons reach their maximum at 7 ms and decrease thereafter (Fig. S2c–g and Fig. S3). Overall, our results indicate that it is advantageous to record [19]F-^{13}C CPMAS spectra with contact times of both 7 and 10 ms. Setting the contact time to 10 ms in the 2D HETCOR experiments

permits detection of cross-peaks corresponding to long-range correlations, as discussed below.

^{1}H-^{13}C and ^{19}F-^{13}C HETCOR: Resonance Assignments and Long-Range Correlations

^{13}C resonances were assigned using 2D ^{1}H-^{13}C and ^{19}F-^{13}C HETCOR spectra and DFT calculations (Fig. S4 of the Supporting Information); all chemical shifts are summarized in Table 2. While most of the ^{13}C signals could be assigned unambiguously based on the calculated frequencies, remaining ambiguities were resolved by analyzing the 2D ^{1}H-^{13}C HETCOR spectra recorded with CP contact times of 0.5 ms and 1.1 ms. Strong peaks present in the 2D HETCOR spectrum recorded with a contact time of 0.5 ms correspond to correlations between carbons and their directly bonded protons, while correlations between carbons and protons separated by two or three bonds appear in the spectrum with 1.1 ms contact time (Fig. 4a). The resonances of the $2CF_3$ and $8CF_3$ groups give rise to intense signals and could be assigned with confidence on the basis of the 2D ^{19}F-^{13}C HETCOR spectrum (contact time of 1 ms), despite their partial overlap with those from C8 and C4a (Fig. 4b). All carbon resonance assignments were validated from the contact-time dependencies of 1D ^{1}H-^{13}C and ^{19}F-^{13}C CPMAS spectra (Fig. S3a, Fig. S4b). For instance, carbon resonances of CF_3 groups as well as C2, C8a and C7, which are all within three bonds of the ^{19}F atoms, are clearly observed in spectra with 1 ms contact time. In contrast, signals corresponding to carbons distant from the fluorine atoms, are relatively weak (C5 and C6) or missing (C4). Similarly, resonances of aromatic carbons, such as C8a, C8 and C4a, have low intensities in the 1 ms ^{1}H-^{13}C CPMAS spectra. Assignments of C15, C16 and C17 resonances are tentative as the corresponding signals partly overlap. To the best of our knowledge, the ^{13}C and ^{19}F chemical shifts of mefloquine have not been reported to date. For several carbon atoms, including C2, C3, C4, C6 and the carbon of $8CF_3$ group, several sets of distinct peaks are observed, which correspond to the crystallographically inequivalent positions of these atoms in the unit cell (Fig. 4c). We also note that the application of ^{1}H and ^{19}F decoupling results in significantly improved spectral resolution, consistent with our observations in the 1D ^{19}F-^{13}C and ^{1}H-^{13}C CPMAS experiments (Fig. 4b–d and Fig. S5 of the Supporting Information).

The ^{19}F-^{13}C multiple-bond correlations were extracted from a series of ^{19}F-^{13}C HETCOR spectra acquired with different contact times. Resonance assignments labeled in Fig. 4b–d were made based on the following considerations: correlations to C3, C4 and the aliphatic carbons are only observed for the ^{19}F signal at 8.8 ppm; therefore, this signal is assigned to the $2CF_3$ group, which is close to the aliphatic carbons. By exclusion, the ^{19}F signal at 15.9 ppm is therefore assigned to the $8CF_3$ group. This assignment is consistent with the DFT calculations, which indicate that the $2CF_3$ group is downfield-shifted and that the ^{19}F chemical shift difference between the $2CF_3$ and $8CF_3$ groups is 8.1 ppm.

To unequivocally distinguish between short- and long-range ^{19}F-^{13}C correlations, we carefully examined the 2D HETCOR spectra acquired with different CP contact times. As can be noted, ^{19}F-^{13}C correlations corresponding to atom pairs separated by 3 or more bonds are only detected when the CP contact time is 7 ms or longer (Fig. 4c and Fig. S5 of the Supporting Information), while ^{19}F-^{13}C correlations involving directly bonded

carbons and carbons within 3 bonds of the fluorine are observed with contact time as short as 1 ms. To observe fluorine correlations with the piperidine ring carbons, such as C12 and C15–17, contact times of 9 ms or longer are necessary. Overall, ^{19}F-^{13}C correlations, corresponding to intra- and intermolecular distances of as long as 6.8 Å were observed. All experimental correlations described above are consistent with the structure of mefloquine and map unambiguously to specific distances (Fig. 4e,f).

^{19}F-^{19}F RFDR: Assignment of Resonances from Crystallographically Inequivalent Sites

At room temperature, the fluorine atoms of the CF_3 groups are expected to give rise to a single ^{19}F resonance due to motional averaging[36,37]. However, multiple ^{19}F chemical shifts were observed for carbon and fluorine atoms of the $2CF_3$ and $8CF_3$ moieties in the ^{19}F-^{13}C HETCOR spectra (Fig. 4b–d), also consistent with the 1D ^{19}F MAS spectra (Fig. 2). The presence of several distinct fluorine signals for each trifluoromethyl group can be explained by the crystal structure of mefloquine: there are three molecules in the unit cell, which result in inequivalent atom positions for the CF_3 groups. To confirm this interpretation, we performed 1D ^{19}F DANTE excitation experiments[38,39], where selective DANTE irradiation was applied at different ^{19}F frequencies (Fig. 5a–d). When DANTE pulses were applied on the $8CF_3$ resonance at 15.9 ppm (Fig. 5c) and $2CF_3$ at 8.8 ppm (Fig. 5d), multiple resolved resonances can be seen at each of the two positions, with resolution increasing with increased DANTE interpulse delay from 2 to 4 rotor cycles. With DANTE selective excitation, at least two signals for the $2CF_3$ moiety and three for the $8CF_3$ moiety were observed. The line widths of the three $8CF_3$ resonances are 0.42 ppm, 0.35 ppm and 0.67 ppm, and the overall width of the $8CF_3$ peak in the absence of the DANTE excitation is 1.13 ppm.

In addition, 2D ^{19}F-^{19}F RFDR spectra were acquired with RFDR mixing times ranging from 1.6 ms to 30.4 ms, resulting in multiple resolved ^{19}F signals for each CF_3 moiety and multiple sets of cross peaks between $2CF_3$ and $8CF_3$ groups (Fig. 5e). Interestingly, the RFDR buildup profiles for the cross peaks are very different. For example, cross peaks labeled "1" and "2" in the spectra were detected with mixing times as short as 1.6 ms, whereas other signals only appear at longer mixing times. To corroborate the presence of these multiple ^{19}F signals in the RFDR spectra, the experiments were performed at MAS frequencies of 40 kHz, 50 kHz and 60 kHz with the RFDR mixing times set to 3.2 ms and 8.0 ms. As shown in Fig. 5g, the spectral resolution increases considerably with the MAS frequency, and the individual peaks become well resolved at 60 kHz. The line widths for the diagonal peaks are 0.35, 0.30, and 0.27 ppm at 40, 50, and 60 kHz, respectively. Furthermore, as a result of enhanced transfer efficiencies at higher spinning frequencies, the peak intensities increase by approximately 25% with every 10 kHz increase in the MAS frequency.

To assign the individual ^{19}F resonances to inequivalent CF_3 groups in the unit cell, DFT calculations were performed for the cluster of 8 molecules shown in Fig. 1b. The resulting calculated shifts for molecules a, b and c are distinct (Table 1), consistent with the experimental findings. The assignments of ^{19}F chemical shifts belonging to inequivalent groups and the corresponding intra-and intermolecular ^{19}F-^{19}F correlations are consistent

with the observed relative cross peak intensities in the RFDR spectra, acquired with different mixing times (Fig. 5e) and the buildup profiles for the different cross peak intensities (Fig. 5f). Specifically, intramolecular correlations between the $2CF_3$ and $8CF_3$ moieties are detected at a mixing time as low as 1.6 ms, whereas correlations for medium- and long-range intermolecular contacts appear only at mixing times of 4.0 ms or longer. Intermolecular $8CF_3$-$8CF_3$ correlations between inequivalent CF_3 groups are strong at the 1.6 ms mixing time, consistent with the short 3.5 Å distances.

Taken together, these above findings indicate that ^{19}F chemical shifts are very sensitive to the slight differences in local environments, allowing for the observation and assignment of inequivalent fluorine positions.

Measurement of Accurate Interfluorine Distances

We determined ^{19}F-^{19}F distances using ^{19}F DANTE-RFDR magnetization exchange profiles. The original version of the experiment by McDermott and coworkers[15] was modified such that a DANTE excitation pulse train was applied on either $2CF_3$ or $8CF_3$. followed by a non-selective homonuclear mixing using RFDR (Fig. 6a). The resulting DANTE-RFDR spectra are shown in Fig. 6b,c and Fig. S8 of the Supporting Information. Increased intensity for the CF_3 signals is clearly observed for increasing RFDR mixing times from 0.8 ms to 16 ms, while without RFDR mixing, no intensity buildup is observed.

^{19}F-^{19}F DANTE-RFDR magnetization exchange profiles (Fig. 6d,e) are clearly dominated by multi-spin effects, similar to our recent findings for crystalline difluorobenzoic acids[24]. Numerical simulations were performed to extract interfluorine distances. In order to account for multi-spin effects, we constructed a large number of 2-spin, 3-spin, 4-spin, 5-spin, and 6-spin systems using combinations of the interfluorine distances from the crystal structure as a set of starting values, which were then varied to assess the resulting error (Fig. S9–10 of the Supporting Information). Clearly, 5 spins are necessary and sufficient to reproduce the experimental magnetization exchange curves (Fig. S9). Analysis of the simulated magnetization exchange profiles for different distance combinations showed that the interfluorine distance between the spin excited by the DANTE sequence and the spin to which the magnetization is transferred dominate the exchange profiles. This is clearly seen from the comparison of the simulation of a 2-spin system with a $2CF_3$-$8CF_3$ distance of 5.4 Å and that of a 5-spin system with four different $2CF_3$-$8CF_3$ distances (with the shortest one being 5.4 Å) and one additional $2CF_3$-$2CF_3$ distance (Fig. S10b). The shortest distance determines the initial buildup rate while the addition of other longer distances influences the detailed oscillation profile after the first intensity maximum. Taking longer distances into account distinctly improves the agreement of the fit with the experimental curve. The overall accuracy of the interfluorine distances extracted from DANTE-RFDR experiments is 0.1–0.2 Å for distances shorter than 7.0 Å and 0.2–0.4 Å for distances in the 7.0 – 11.0 Å range, similar to our recent findings for difluorobenzoic acids[24].

We also carried out simulations using several 5-spin systems in which the intramolecular distance between $2CF_3$ and $8CF_3$ groups as well as several intermolecular distances were included. Excellent agreement is observed between the simulated and experimental curves if intra- and intermolecular ^{19}F-^{19}F distances shorter than 11 Å are taken into account

(Fig. 6d–e). The best agreement for the 2CF$_3$ exchange curve is observed for a 2CF$_3$-8CF$_3$ intramolecular distance of 5.5 6, and intermolecular distances of 8.0 Å, 9.9 Å and 10.5 Å, with an added 8CF$_3$-8CF$_3$ distance of 7.0 Å included as well. Likewise, the best agreement for 8CF$_3$ group was obtained with identical 2CF$_3$-8CF$_3$ distances and two additional intermolecular 2CF$_3$-2CF$_3$ distances of 7.4 Å and 10.6 Å. Remarkably, the 2CF$_3$-2CF$_3$ distance determined by the simulation is 7.2 6, only 0.2 6 different from the actual distance of 7.4 Å in the X-ray crystal structure. Overall, all distances determined by the simulations are consistent with ^{19}F-^{1}9F distances within the cluster of CF$_3$ groups in the crystal lattice.

DISCUSSION

While DANTE-RFDR protocols for accurate interfluorine distance measurements have been applied here for mefloquine, whose X-ray structure is known, it is important to point out that the present ^{19}F fast MAS NMR crystallography approach is applicable for analysis of any crystalline fluorinated solid of unknown structure. By integrating the information from ^{19}F-^{19}F DANTE-RFDR magnetization exchange curves with ^{19}F, ^{13}C, and ^{1}H chemical shifts and various internuclear correlations, structures can be determined without the need for single crystal diffraction data, as has been shown for other systems[40]. In our earlier study, we have demonstrated that an unbiased grid search could be successfully applied to derive distance distributions from the experimental ^{19}F-^{19}F DANTE-RFDR data in 2,5-difIuorobenzoic acid, and that five-spin systems are sufficient to reproduce the magnetization exchange profiles for many organic crystals with extensive coupling networks[24]. In principle, the experiments discussed in this work can also be applied to amorphous systems, albeit with likely lower information content due to their associated structural heterogeneity and broader line widths.

Magnetic field strength is an important consideration for the ^{19}F fast MAS NMR experiments described here, given that the ^{19}F chemical shift range and chemical shift anisotropy (CSA) are proportional to the field strength. We see clear benefits of higher magnetic fields for fast MAS ^{19}F spectroscopy: going from 11.7 T to 16.4 T to 19.9 T in experiments on mefloquine results in increased sensitivity and resolution. Naturally, higher fields are generally advantageous when multiple fluorine sites with similar isotropic chemical shifts are present in the system. This is certainly seen for mefloquine, investigated here, but applies also to fluorinated tryptophans,[25] difluorobenzoic acids[24] as well as HIV-1 CA protein assemblies labeled with 5F-Trp residues,[26] which we reported on previously. At this juncture it is important to note is that for many fluorinated organic moieties the ^{19}F CSA lie in the 40–80 ppm range, which can be efficiently averaged out upon spinning at MAS frequencies exceeding 40 kHz, even at high magnetic fields (19.9 T).

As to the choice of MAS frequency, as observed here for mefloquine and in previous studies,[24–26] spinning frequencies of at least 40 kHz are required to obtain well-resolved spectra in the absence of decoupling, with further gains in sensitivity and resolution seen at 60 kHz MAS. As shown here, spinning frequencies of 40 kHz and higher were critical for acquiring high-resolution/high-sensitivity ^{19}F-^{13}C/^{13}C-^{19}F and ^{19}F-^{1}H/^{1}H-^{19}F HETCOR spectra of mefloquine. Even further gains in sensitivity and resolution are anticipated at ultrafast MAS frequencies of 111 kHz and above.

CONCLUSIONS

A fast MAS ^{19}F NMR approach for the structural characterization of fluorine-containing natural abundance pharmaceutical compounds is presented. [19]F-^{13}C HETCOR and [19]F-^{19}F RFDR experiments together with DFT calculations readily permit assignments and identification of inequivalent sites in the crystal. Accurate interfluorine distances are obtained from DANTE-RFDR magnetization exchange profiles and multi-spin numerical simulations. The NMR crystallography approach presented here can be extended to pharmaceuticals of unknown structures and is broadly applicable to organic and biological molecules, including crystalline organic compounds, peptides and proteins as well as protein assemblies possessing long-range order, such as assemblies of virus proteins and amyloid fibrils.

MATERIALS AND METHODS

Chemicals

Natural abundance mefloquine hydrochloride was purchased from Acros Organics and used without further recrystallization. For MAS NMR experiments, sample amounts were as follows: 3 mg (1.3 mm rotor for measurements at 11.7 T), 3.7 mg (1.3 mm rotor for measurements at 14.1 T), 9.5 mg (1.6 mm rotor for measurements at 16.4 T), and 13.5 (1.9 mm rotor for measurements at 19.9 T).

MAS NMR spectroscopy

[19]F and ^{13}C-detected experiments were performed on a 20.0 T narrow bore Bruker AVANCE III spectrometer outfitted with a 1.9 mm HX MAS probe. The Larmor frequencies were 850.4 MHz for ^{1}H, 800.1 MHz for ^{19}F and 213.8 MHz for [13]C. For all ^{19}F-detected experiments, the ^{1}H channel was tuned to [19]F. All MAS NMR spectra were acquired at a MAS frequency of 40 kHz maintained within ± 10 Hz by Bruker MAS III controller. The sample temperature was calibrated with KBr as an external temperature sensor and was maintained at 12.0±0.3 °C by a Bruker variable temperature controller. Typical 90° pulse lengths were 1.5 μs for ^{1}H, 1.1 is for ^{19}F and 3.0 μs for [13]C. [19]F chemical shifts were referenced externally with respect to those of trifluoroacetic acid (100 μM solution in 25 mM sodium phosphate buffer, pH 6.5) used as an external reference (0 ppm), which relates to other commonly used reference standards as: neat trifluoroacetic acid (−2.8 ppm), trichloro-fluoro-methane (73.55 ppm), Teflon (−48.45 ppm). [13]C chemical shifts were referenced externally to adamantane.

The [19]F-^{13}C cross-polarization was performed with a linear amplitude ramp of 70–100 % on ^{13}C and the center of ramp was Hartmann-Hahn matched at the first or second spinning sideband; the carrier frequency on ^{13}C was set to 100 ppm. For optimization of [19]F-^{13}C CP, ^{19}F rf fields of 15, 25, 30, 35, 45 and 55 kHz were applied, and Hartmann-Hahn matched at 1~3 times of the spinning frequency (v_r). Zero quantum (ZQ) or double quantum (DQ) CP was matched with the ^{19}F rf field fixed while the ^{13}C rf field was systematically varied over a range of 0 kHz to 75 kHz. [19]F-^{13}C CPMAS spectra were acquired with 512 scans and CP

contact times varied systematically from 1.0 ms to 10.0 ms; the rf fields were 15 kHz for ^{19}F and 25 kHz (DQ-CP) or 55 kHz (ZQ-CP) for ^{13}C. For 2D ^{19}F-^{13}C HETCOR experiments, the CP contact times were 1.0, 7.0 and 10.0 ms; both DQ-CP and ZQ-CP conditions were used; 38 complex points were acquired in t_2 dimension. The carrier frequencies in ^{13}C were set to 100.0 ppm. In several experiments, π-pulse ^{19}F decoupling at RF field of 208 kHz was applied during evolution in ^{13}C dimension. A recycle delay of 6.0 s was used for all experiments.

For ^{1}H-^{13}C CPMAS experiments, the ^{1}H-^{13}C cross polarization was performed with a linear ramp; the ^{1}H and ^{13}C RF fields were at 13 kHz and 28 kHz, respectively; the typical CP contact times were 0.5–1.4 ms. 2D ^{1}H-^{13}C HETCOR spectra with 0.5 ms and 1.1 ms CP contact were acquired with 448 and 384 transients, respectively; 80 complex points were collected in the indirect dimension.

2D ^{19}F-^{19}F RFDR spectra were acquired without decoupling with RFDR mixing times of 1.6 ms, 4 ms, 8 ms, 12 ms, 20 ms and 30.4 ms. The typical length of the RFDR π pulse was 8.3 μs and a XY-16 phase cycle was used during the RFDR mixing. For each ^{19}F-^{19}F spectrum, the data were collected with 120 complex points in t_2 dimension using States-TPPI phase sensitive detection; 16 transients were averaged for each FID. The 1D ^{19}F DANTE spectra were acquired with 16 scans; 22 0.1-μs DANTE pulses were applied at 8.8 ppm and 15.9 ppm for selective irradiation of 2CF$_3$ and 8CF$_3$ signals, respectively. The DANTE interpulse delay was set to 4 rotor cycles. The recycle delay was 5.0 s.

^{19}F-detected single pulse excitation spectra were also acquired on a 11.7 T wide bore Bruker AVANCE III spectrometer outfitted with a 1.3 mm HFX MAS probe. The Larmor frequencies were 500.13 MHz for ^{1}H and 470.59 MHz for ^{19}F. The MAS frequencies were 10, 40, and 60 kHz maintained within ±10 Hz by Bruker MAS III controller. Spinal-64[41] (10 kHz MAS) or swept-frequency two-pulse phase modulation (SW$_f$-TPPM)[42] heteronuclear decoupling sequences were applied with the ^{1}H RF field strengths of 90 kHz, 15 kHz, and 10 kHz for the MAS frequencies of 10 kHz, 40 kHz, and 60 kHz, respectively. ^{19}F 90° pulse length was 2.45 μs. The recycle delay was 6.0 s.

Additional 2D ^{19}F-^{19}F RFDR spectra were recorded 14.1 T, on a Magnex narrow-bore magnet interfaced with a Bruker AVIII HD spectrometer, and outfitted with a 1.3 mm Bruker HCN MAS probe. The H channel was tuned to the ^{19}F Larmor frequency of 564.35 MHz and the typical ^{19}F 90° pulse length was 3.3 μs for. ^{19}F-^{19}F RFDR spectra were recorded for MAS frequencies of 40 kHz, 50 kHz and 60 kHz with RFDR mixing times of 3.2 ms and 8.0 ms, 16 transients were averaged and the recycle delay was 2.0 s. The pulse length for the DANTE selective excitation pulses was 0.1 μs. The interpulse delay was set to 2 rotor cycles. The DANTE-RFDR magnetization exchange curves were recorded with RFDR mixing times of 0.8, 1.6, 3.2, 4.0, 5.6, 8.0, 12.0, 16.0, 21.6, 26.4, and 30.4 ms; (XY8)$^1_4$ phase cycle[43] was applied during the RFDR mixing.

Supplemental ^{19}F-^{13}C CPMAS and HETCOR NMR spectra were acquired on a 16.4 T Bruker spectrometer equipped with a PhoenixNMR 1.6 mm HFX MAS probe at a MAS frequency of 40 kHz. The Larmor frequencies were 700.1 MHz for ^{1}H, 658.8 MHz for ^{19}F

and 176.0 MHz for ^{13}C. The typical 90° pulse lengths were 2.5 μs for ^{1}H, 2.0 μs for ^{19}F, and 1.97 μs for ^{13}C. The ^{19}F-^{13}C CP contact time was 7.0 ms. ^{1}H and ^{19}F decoupling was applied simultaneously during the t_2 evolution in the ^{13}C dimension. ^{1}H decoupling used low-power XiX[35] with an rf field of 12.5 kHz. For ^{19}F decoupling, a π-pulse with the rf field of 125 kHz was applied every rotor period. A spin echo ^{1}H π-pulse was applied in the center of the t_1 evolution in the ^{19}F dimension to refocus the ^{1}H offset and heteronuclear coupling. The recycle delay was 3 s.

All spectra were processed in TopSpin 4.0 and analyzed with Sparky[44] and Mnova.

Numerical simulations

The DANTE-RFDR magnetization exchange curves were simulated using SIMPSON[45] (version 3.1.0). In the multi-spin simulation, the magnetization exchange was followed starting from the non-selectively irradiated spin and the evolution of the spin to which the magnetization is transferred was performed from l_{2x} to $-l_{1z}$. The experimental decay curves of the signals that are selectively excited by the DANTE pulse are scaled to 1 and the experimental buildup curves of the nonselective signals are scaled to 0. The simulated DANTE-RFDR exchange curves were rescaled to match the experimental intensities. The example simulation script is present in the Supporting Information.

DFT calculations

^{19}F and ^{13}C magnetic shielding tensor calculations were carried out in Gaussian 09 (Revision D.01)[46]. Molecular clusters of mefloquine comprising 8 molecules were generated from the crystal structures by Pymol[47]. All-atom geometry optimizations were performed using a M06 functional with the cc-pVTZ basis set and geometry-optimized models were used for magnetic shielding tensor calculations at the same level of theory. The chemical shifts were referenced by converting absolute magnetic shielding constants, σ, into absolute chemical shifts, using the relation $δ_i = σ_{ref} - σ_i$ with the value of σref determined by linear regression between calculated and experimental shifts[48].

Supplementary Material

Refer to Web version on PubMed Central for supplementary material.

REFERENCES

(1). Purser S; Moore PR; Swallow S; Gouverneur V Chem. Soc. Rev. 2008, 37, 320–330. [PubMed: 18197348]

(2). Zhou Y; Wang J; Gu Z; Wang S; Zhu W; Luis Acena J; Soloshonok VA; Izawa K; Liu H Chem. Rev. 2016, 116, 422–518. [PubMed: 26756377]

(3). Mei HB; Han JL; Fustero S; Medio-Simon M; Sedgwick DM; Santi C; Ruzziconi R; Soloshonok VA Chem. - Eur. J. 2019, 25, 11797–11819. [PubMed: 31099931]

(4). Inoue M; Sumii Y; Shibata N ACS Omega 2020, 5, 10633–10640. [PubMed: 32455181]

(5). Gakh YG; Gakh AA; Gronenborn AM Magn. Reson. Chem. 2000, 38, 551–558.

(6). Gerig JT httDS://Www.biODhvsics.oro/Portals/0/BPSAssets/Articles/oerio.Ddf 2001.

(7). Zhao Y; Markopoulos G; Swager TM J. Am. Chem. Soc. 2014, 136, 10683–10690. [PubMed: 25051051]

(8). Tengel T; Fex T; Emtenas H; Almqvist F; Sethson I; Kihlberg J Org. Biomol. Chem. 2004, 2, 725–731. [PubMed: 14985813]

(9). Norton RS; Leung EWW; Chandrashekaran IR; MacRaild CA Molecules 2016, 21. [PubMed: 28035966]

(10). Lu MM; Ishima R; Polenova T; Gronenborn AM J. Biomol. NMR 2019, 73, 401–409. [PubMed: 31435857]

(11). Matei E; Gronenborn AM Angewandte Chemie (International ed. in English) 2016, 55, 150–154. [PubMed: 26510989]

(12). Sharaf NG; Gronenborn AM Methods in enzymology 2015, 565, 67–95. [PubMed: 26577728]

(13). Boeszoermenyi A; Chhabra S; Dubey A; Radeva DL; Burdzhiev NT; Chanev CD; Petrov OI; Gelev VM; Zhang M; Anklin C; Kovacs H; Wagner G; Kuprov I; Takeuchi K; Arthanari H Nat. Methods 2019, 16, 333–340. [PubMed: 30858598]

(14). Danielson MA; Falke JJ Annu. Rev. Biophys. Biomol. Struct. 1996, 25, 163–195. [PubMed: 8800468]

(15). Gilchrist ML; Monde K; Tomita Y; Iwashita T; Nakanishi K; McDermott AE J. Magn. Reson. 2001, 152, 1–6. [PubMed: 11531358]

(16). Lu X; Skomski D; Thompson KC; McNevin MJ; Xu W; Su Y Anal. Chem. 2019, 9f, 6217–6224. [PubMed: 30990668]

(17). Kozorog M; Sani M-A; Separovic F; Anderluh G Chemistry — A European Journal 2018, 24, 14220–14225. [PubMed: 29979814]

(18). Roos M; Mandala VS; Hong MJ Phys. Chem. B 2018, f22, 9302–9313.

(19). Roos M; Wang T; Shcherbakov AA; Hong MJ Phys. Chem. B 2018, 122, 2900–2911.

(20). Shcherbakov AA; Hong MJ Biomol. NMR 2018, 71, 31–43.

(21). Shcherbakov AA; Roos M; Kwon B; Hong MJ Biomol. NMR 2020, 74, 193–204.

(22). Su YC; DeGrado WF; Hong MJ Am. Chem. Soc. 2010, 132, 9197–9205.

(23). Su YC; Doherty T; Waring AJ; Puchala P; Hong M Biochemistry 2009, 48, 4587–4595. [PubMed: 19364134]

(24). Fritz M; Kraus J; Quinn CM; Yap GPA; Struppe J; Sergeyev IV; Gronenborn AM; Polenova TJ Phys. Chem. B 2019, 123, 10680–10690.

(25). Lu M; Sarkar S; Wang M; Kraus J; Fritz M; Quinn CM; Bai S; Holmes ST; Dybowski C; Yap GPA; Struppe J; Sergeyev IV; Maas W; Gronenborn AM; Polenova TJ Phys. Chem. B 2018, 122, 6148–6155.

(26). Wang M; Lu M; Fritz MP; Quinn CM; Byeon I-JL; Byeon C-H; Struppe J; Maas W; Gronenborn AM; Polenova T Angew. Chem. Int. Ed. 2018, 57, 16375–16379.

(27). Wi S; Sinha N; Hong MJ Am. Chem. Soc. 2004, 126, 12754–12755.

(28). Abraham A; Crull G Mol. Pharmaceutics 2014, 11, 3754–3759.

(29). Lu X; Huang C; Li M; Skomski D; Xu W; Yu L; Byrn SR; Templeton AC; Su YJ Phys. Chem. B 2020, 124, 5271–5283.

(30). Lu M; Wang M; Sergeyev IV; Quinn CM; Struppe J; Rosay M; Maas W; Gronenborn AM; Polenova TJ Am. Chem. Soc. 2019, 141, 5681–5691.

(31). Karle JM; Karle IL Antimicrob. Agents Chemother. 2002, 46, 1529–1534. [PubMed: 11959592]

(32). Censi R; Di Martino P Molecules 2015, 20, 18759–18776. [PubMed: 26501244]

(33). Gupta H; Kumar S; Roy SK; Gaud RS J Pharm Bioallied Sci 2010, 2, 2–7. [PubMed: 21814422]

(34). Liu SF; Schmidt-Rohr K Macromolecules 2001, 34, 8416–8418.

(35). Ernst M; Samoson A; Meier BH J. Magn. Reson. 2003, 163, 332–339. [PubMed: 12914849]

(36). Grage SL; Ulrich AS J. Magn. Reson. 2000, 146, 81–88. [PubMed: 10968960]

(37). Wang XL; Mallory FB; Mallory CW; Beckmann PA; Rheingold AL; Francl MM J. Phys. Chem. A 2006, 110, 3954–3960. [PubMed: 16539417]

(38). Bodenhausen G; Freeman R; Morris GA J. Magn. Reson. 1976, 23, 171–175.

(39). Morris GA; Freeman RJ Magn. Reson. 1978, 29, 433–462.

(40). Martineau C; Senker J; Taulelle F Annual Repods on NMR Spectroscopy 2014, 82, 1–57.

(41). Fung BM; Khitrin AK; Ermolaev K J Magn Reson 2000, 142, 97–101. [PubMed: 10617439]

(42). Augustine C; Kurur ND J. Magn. Reson. 2011, 209, 156–160. [PubMed: 21306928]

(43). Shen M; Hu B; Lafon O; Trebosc J; Chen Q; Amoureux J-PJ Magn. Reson. 2012, 223, 107–119.

(44). Goddard TD; Kneller DG University of California, San Francisco.

(45). Bak M; Rasmussen JT; Nielsen NC J. Magn. Reson. 2000, f47, 296–330. [PubMed: 11097821]

(46). Frisch MJ; Trucks GW; Schlegel HB; Scuseria GE; Robb MA; Cheeseman JR; Scalmani G; Barone V; Mennucci B; Petersson GA; Nakatsuji H; Caricato M; Li X; Hratchian HP; Izmaylov AF; Bloino J; Zheng G; Sonnenberg JL; Hada M; Ehara M, et al. Gaussian, Inc., Wallingford CT 2009.

(47). Schrodinger, LLC.

(48). Baias M; Dumez J-N; Svensson PH; Schantz S; Day GM; Emsley LJ Am. Chem. Soc. 2013, 135, 17501–17507.
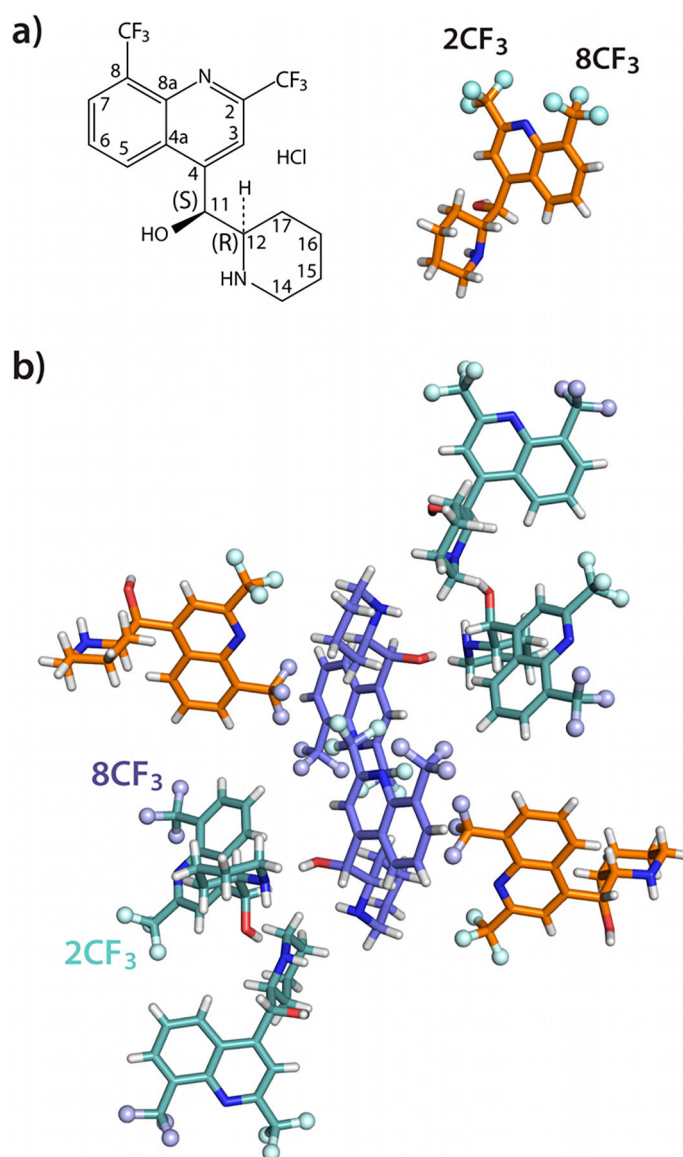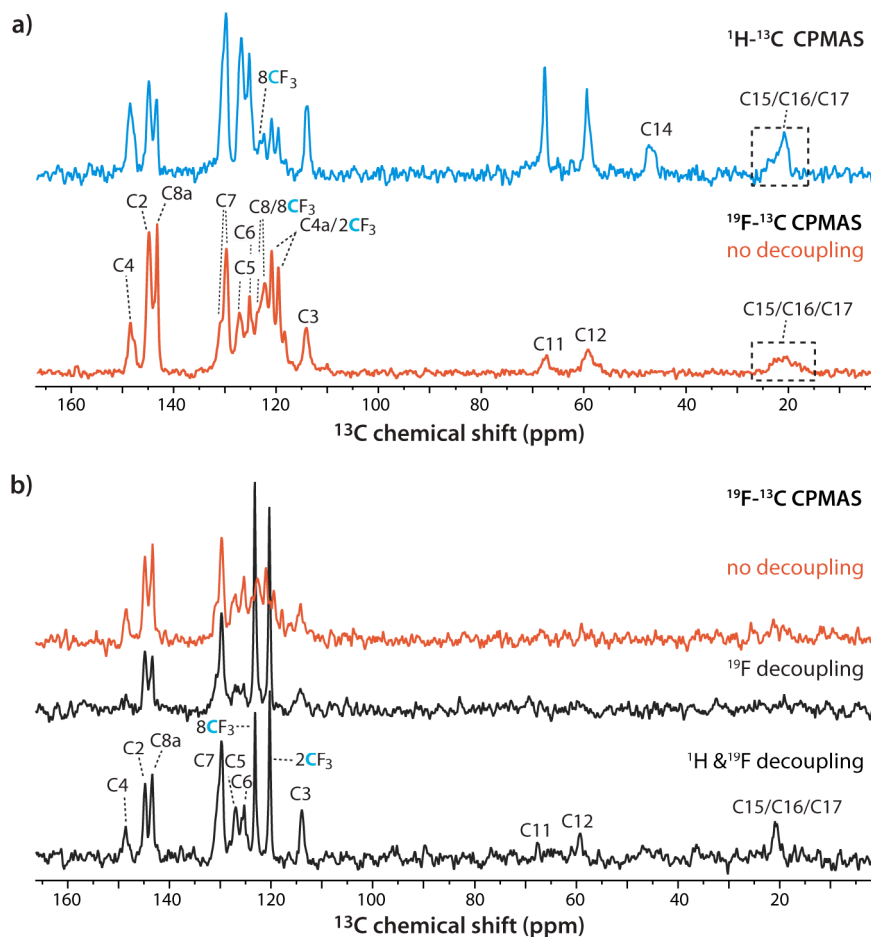
Figure 1.

a) Chemical and 3D structure of mefloquine. b) Arrangement of mefloquine molecules in the crystal. The three types of inequivalent molecules are colored in purple, orange and cyan. The fluorine atoms are shown as spheres. The 8CF$_3$ and 2CF$_3$ groups are colored in light purple and light cyan, respectively.
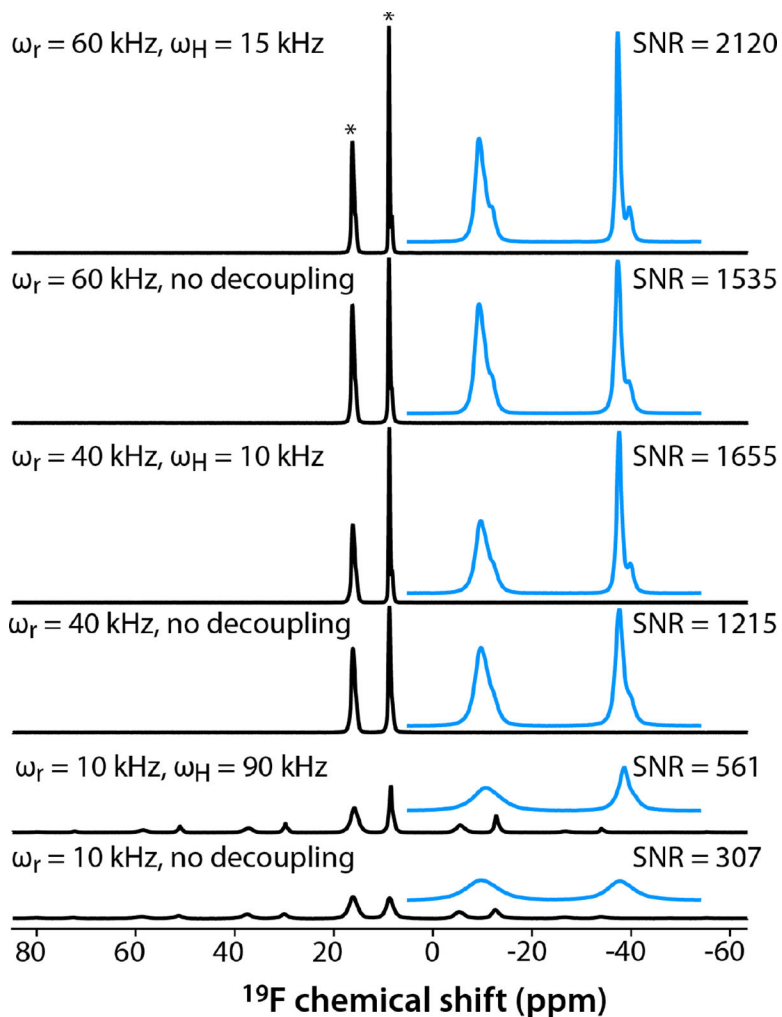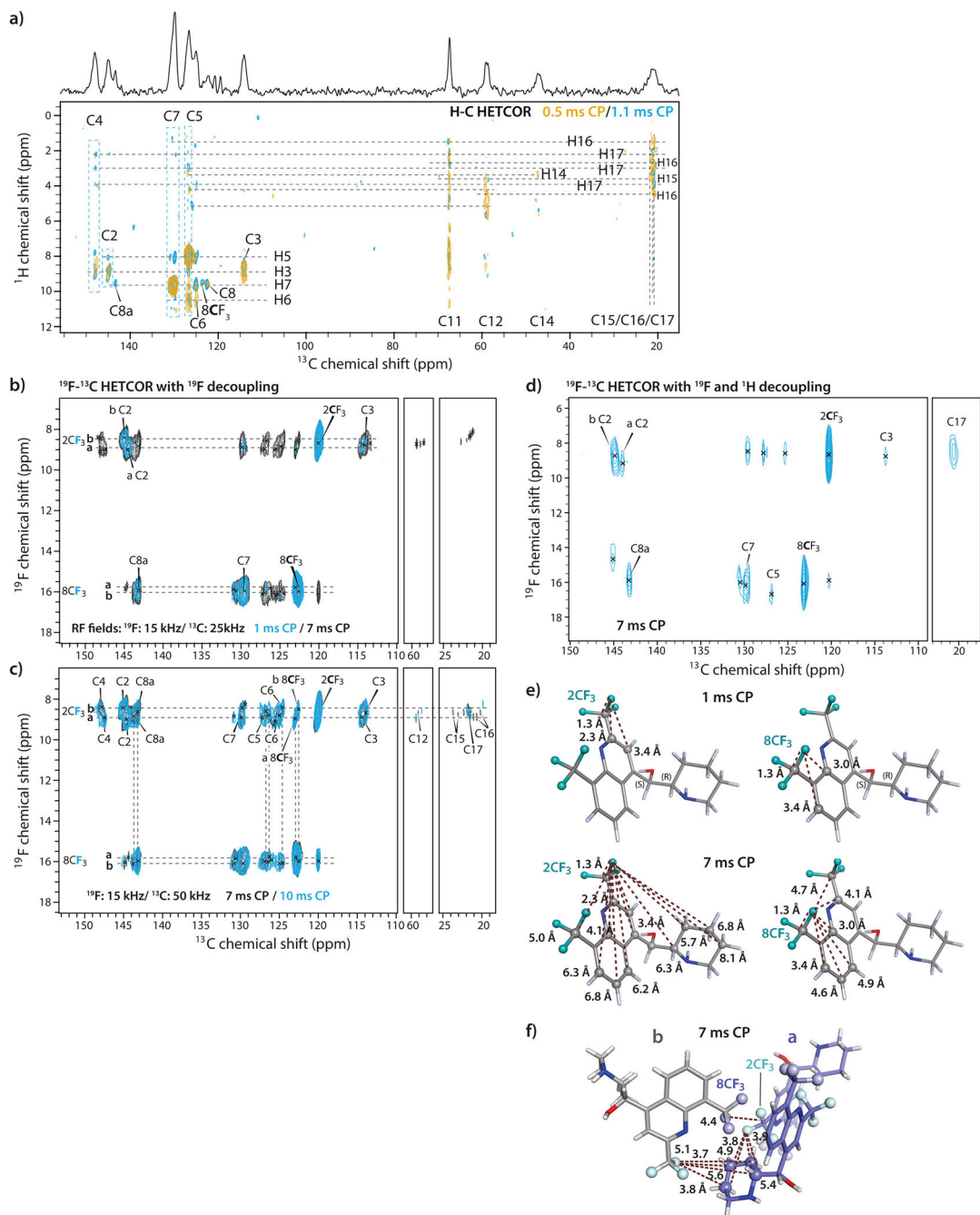
Figure 2.

^{19}F MAS spectra of mefloquine acquired at MAS frequencies of 60 kHz (top two traces), 40 kHz (middle two traces), and 10 kHz (bottom two traces), with or without SW$_f$-TPPM ^{1}H decoupling at the RF field strength, as indicated next to each spectrum. The blue traces are expansions around the isotropic peaks (marked with asterisks). The signal-to-noise ratios (SNR) are indicated next to each trace. The spectra were acquired at 11.7 T using a 1.3 mm HFX MAS probe, averaging 32 scans.

Figure 3.

a) ^{1}H-^{13}C and ^{19}F-^{13}C CPMAS spectra of mefloquine. The spectra were acquired at 20.0 T using a 1.9 mm HX MAS probe, averaging 512 scans and 1920 scans and CP contact time of 1.4 and 6 ms, respectively. The ^{19}F-^{13}C spectrum was acquired without decoupling. b) ^{19}F-^{13}C CPMAS spectra of mefloquine without decoupling acquired (top trace), with ^{19}F decoupling (middle trace), and with ^{1}H and ^{19}F decoupling (bottom trace). The spectra were acquired at 16.4 T using a 1.6 mm HFXY MAS probe, averaging 512 scans; the CP contact time was 7 ms. The MAS frequency was 40 kHz in every case. Assignments for individual carbon signals are shown in the different spectra.

Figure 4.

a) 2D ^{1}H-^{13}C HETCOR spectra acquired with CP contact times of 0.5 ms (yellow) and 1.1 ms (blue). b)-d) 2D ^{19}F-^{13}C HETCOR spectra acquired with CP contact times of 1ms and 7 ms (b), 7 ms and 10 ms with ^{19}F decoupling (c), and with a CP contact time of 7 ms with ^{1}H and ^{19}F decoupling (d). The rf fields for ^{19}F and ^{13}C were 15 kHz and 25 kHz (b) or 50 kHz (c), respectively. The spectrum shown in d) was acquired at 16.4 T with 8 scans. All other spectra were acquired at 20.0 T with 256 scans. The MAS frequency was 40 kHz. Carbon assignments are indicated. e) Short- and long-range intramolecular ^{19}F-^{13}C distances
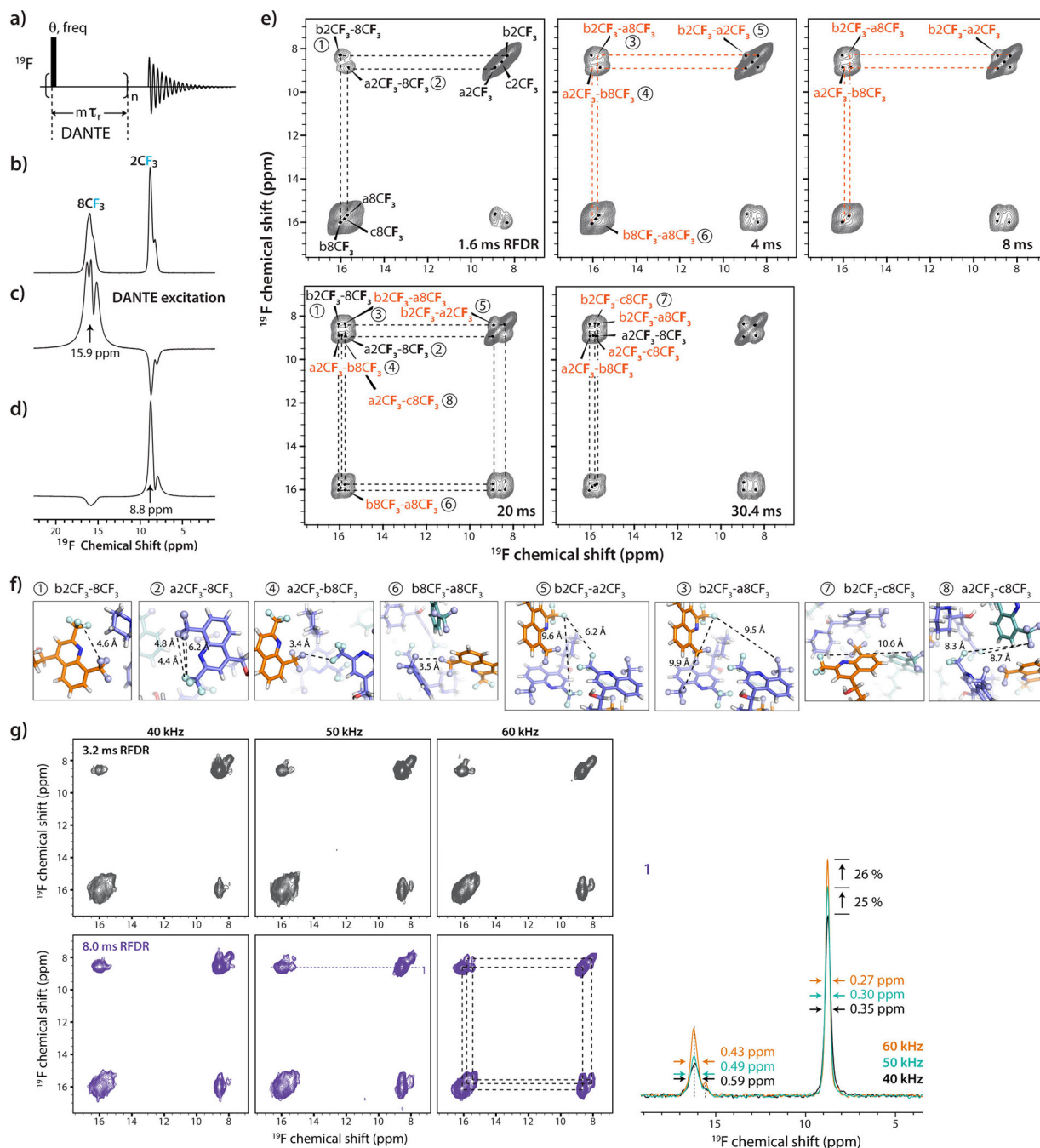
in the mefloquine crystal structure consistent with correlations in the HETCOR spectra for 1ms and 7 ms contact times. f) Intermolecular ^{19}F-^{13}C distances < 6 Å in the crystal lattice.
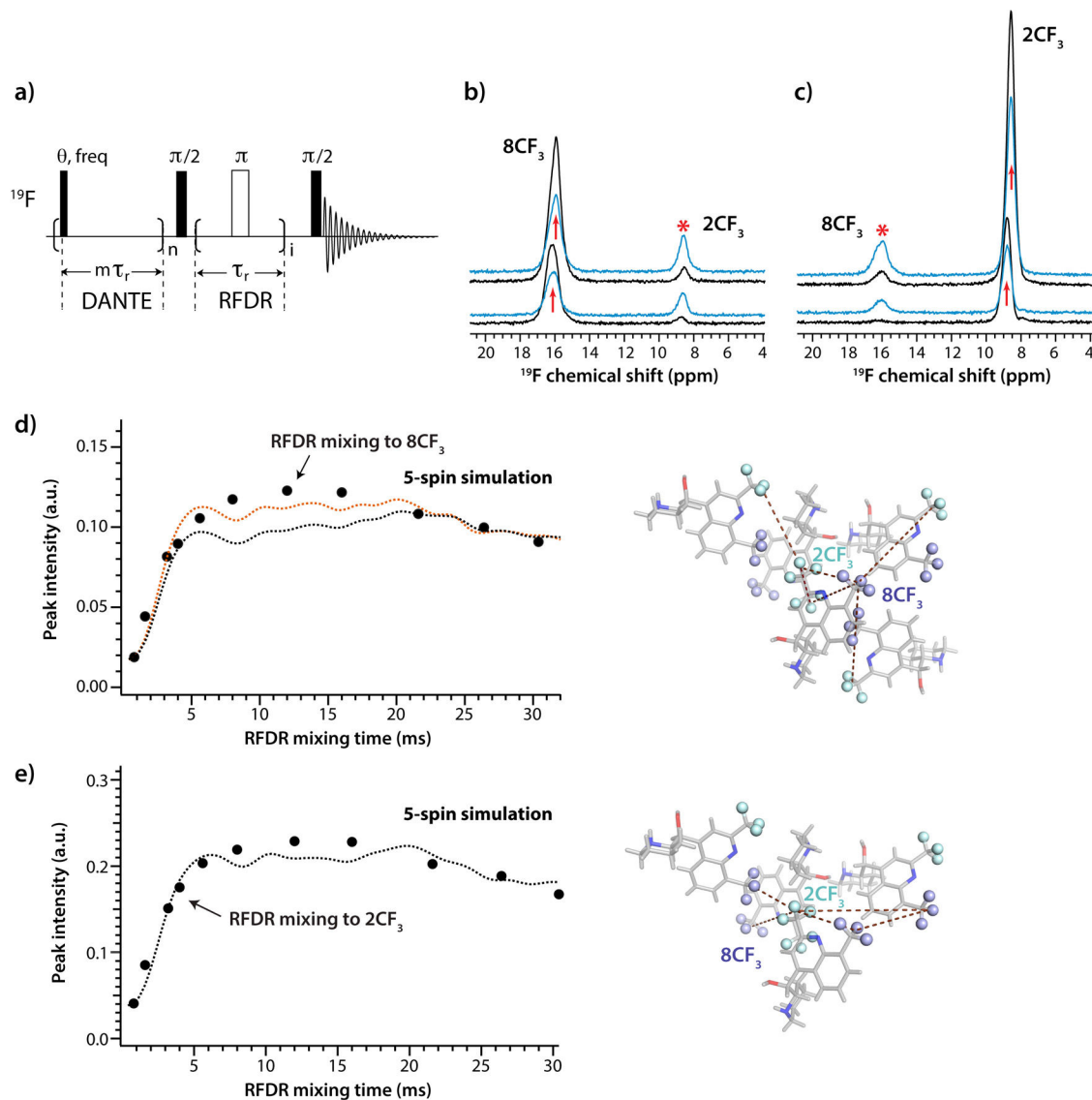
Figure 5.

a)-d) Pulse sequence (a), 1D ^{19}F MAS NMR spectrum (b) with ^{19}F DANTE selective excitation of the 8CF$_3$ resonance at 15.9 ppm (c) and 2CF$_3$ resonance at 8.8 ppm (d). Spectra were acquired at 20.0 T, with a MAS frequency of 40 kHz, averaging 16 scans and a DANTE interpulse delay of 4 rotor periods. e) 2D ^{19}F-^{19}F RFDR spectra with increased mixing times from 1.6 ms to 30.4 ms. Intramolecular and intermolecular correlations are shown in black and orange, respectively. f) The intra- and intermolecular interfluorine distances in crystal structure of mefloquine. The notation for each ^{19}F-^{19}F distance is

identical to the corresponding correlation 2D ^{19}F-^{19}F RFDR spectra. The fluorine atoms in CF$_3$ groups are shown in light cyan. g) Left panels: 2D ^{19}F-^{19}F RFDR spectra acquired at the MAS frequencies of 40 kHz (left), 50 kHz (middle), and 60 kHz (right). The RFDR mixing times were 3.2 ms (gray) and 8.0 ms (dark purple). Right panel: the 1D traces of the 2D spectra with 8 ms RFDR mixing extracted at 8.61 ppm for MAS frequencies of 40 kHz (cyan), 50 kHz (black) and 60 kHz (orange). The peak widths are indicated in the slices.

Figure 6.
a) Pulse sequence for the 1D RFDR experiment with ^{19}F DANTE-excitation. b),c) 1D ^{19}F-^{19}F DANTE-RFDR spectra with DANTE 90° selective excitation applied to the ^{19}F resonances of $2CF_3$ (b) and $8CF_3$ (c), respectively. Spectra acquired with RFDR mixing times of 1.6 ms and 8.0 ms are shown in black and blue, respectively. The position of the DANTE excitation is shown with arrows and the resonances to which the magnetization was transferred by asterisks. d),e) Left: Experimental and simulated ^{19}F-^{19}F DANTE-RFDR magnetization exchange curves for the $8CF_3$ (d) and $2CF_3$ (e) resonances. The experimental data points are shown as black circles, the simulated curves, as dashed lines. In d), the $2CF_3$ spins were excited by DANTE pulses and magnetization was transferred to the $8CF_3$ spins during RFDR mixing period. In e), DANTE excitation was applied to the $8CF_3$ resonances and magnetization was transferred to the $2CF_3$ groups. Errors in the data points as defined by the standard deviation of the noise in a region of over 10 ppm are smaller than the size of the circles. The RMSDs of the simulated DANTE-RFDR magnetization exchange curves

(dashed lines) are 0.008 (orange, the $2CF_3 — 2CF_3$ distance is 7.2 Å) and 0.014 (black, the $2CF_3 — 2CF_3$ distance is 7.4 Å) for $8CF_3$ (d) and 0.014 for $2CF_3$ (e). Right: Sets of interfluorine distances used in the 5-spin simulations, see also Table 3.

Table 1.

MAS NMR Experimental and DFT Calculated ^{19}F Isotropic Chemical Shifts for Mefloquine

Crystallographically inequivalent molecules	Functional group	δ_{iso} (ppm) MAS NMR	δ_{iso} (ppm) DFT
a	2C**F**$_3$	8.8	7.4
a	8C**F**$_3$	15.6	15.5
b	2C**F**$_3$	8.2	1.5
b	8C**F**$_3$	16.1	16.1
c	2C**F**$_3$	8.6	1.6
c	8C**F**$_3$	15.8	14.9

Table 2.

MAS NMR Experimental and DFT Calculated ^{13}C Isotropic Chemical Shifts and Interatomic Distances in Mefloquine

Carbon atom	δ^{13}C (ppm) MAS NMR		δ^{13}C (ppm) DFT	Distance to ^{19}F (Å)	
	a	b		2CF$_3$	8CF$_3$
C4	147.5	148	157.2	4.5[*]	5.2
C2	144.3	145	150.9	2.3	4.1
C8a	143.6	143.2	146.7	4.1	3
C7	129.7		134.3	6.3	3.4
C5	126.8		132.4	6.2	4.9
C6	125.2	124.7	128.7	6.8	4.6
8CF$_3$	123.0	122.6	126.2	5	1.3
C8	122.2#		126.6	5	2.4
C4a	120.8#		125.1	4.9	4.3
2CF$_3$	120.1		122.4	1.3	4.7
C3	114.3	114.1	114.2	3.4	5.2
C11	67.7		71.7	5.8	6.7
C12	59.3	58.8	58.4	6.3	7
C14	47		44.9	8.5	9
C15	23.1, 22.4	(22.3–23.6)	24.8	8.1	9.1
C17	21.7, 21.4	(21.3–22.0)	21.4	5.7	7
C16	21.0, 20.1	(19.8–20.9)	20.3	6.8	7.7

[*]Resonances were assigned on the basis of ^{19}F-^{13}C CPMAS, ^{1}H-^{13}C CPMAS and ^{19}F-^{13}C HETCOR spectra. Correlations detected in 2D FC-HETCOR with the 7.0 ms CP contact time are highlighted in green and those only detected with the 1ms CP contact in light green.

Table 3.

Sets of Interfluorine Distances for the 5-spin Simulations and in the X-ray Crystal Structure

Type of Interfluorine Distances	Simulation	X-ray
$2CF_3 - 8CF3$	5.5 Å	5.5 Å
	8.0 Å	8.0 Å
	9.9 Å	9.9 Å
	10.5 Å	10.5 Å
$2CF_3 - 2CF_3$ (Simulation for $8CF_3$ resonance)	7.4 Å / 7.2 Å	7.4 Å
	10.6 Å	
$8CF_3 - 8CF_3$ (Simulation for $2CF_3$ resonance)	7.0 Å	7.0 Å